AIChE

Dispensing of Rheologically Complex Fluids: The Map of Misery

Christian Clasen, Paul M. Phillips, Ljiljana Palangetic, and Jan Vermant
Dept. of Chemical Engineering, Katholieke Universiteit Leuven, W. De Croylaan 46, B-3001 Leuven, Belgium

DOI 10.1002/aic.13704
Published online December 7, 2011 in Wiley Online Library (wileyonlinelibrary.com).

Rheological effects may complicate the dispensing of complex fluids, when compared to their Newtonian counterparts. In this work, fluids with tailored rheological properties have been studied using high-speed video-microscopy. The level of viscosity, the degree of shear thinning, and the elasticity have been varied independently. At low-flow rates, droplets are formed that pinch off. The drop volumes, breakup mechanisms, and times have been identified. At higher-flow rates, a continuous jet is observed, with the transition depending on the rheology of the dispensed fluid. The relevant nondimensional groups are the Ohnesorge, Deborah, and elasto-capillary number, for when viscosity, inertia, or elastic forces dominate flow. In each of these cases, the transition between dripping and jetting dispensing occurs, controlled by a critical Weber, capillary, and Weissenberg number, respectively. This set of six nondimensional groups can be used to construct an operating space and map out areas of potential problems. © 2011 American Institute of Chemical Engineers
AIChE J, 58: 3242–3255, 2012
Keywords: complex fluids, fluid mechanics, rheology, dispensing, capillary thinning

Introduction

Accurate dispensing of complex fluids is relevant in a number of industrial applications, for example, when dosing consumer products and pharmaceutical dispersions, or in printing applications. Although dispensing a desired volume (or mass) of a Newtonian liquid through an orifice is generally not problematic,[1] non-Newtonian or viscoelastic behavior may lead to unexpected results.[2–5] The traditional way to circumvent this is to calibrate a fluids handler for each individual fluid at all required flow rates and desired dispensing volumes.[6] Although this is a widely used method, it is time consuming and small changes in operating conditions may lead to large differences due to the inherent nonlinear fluid response.

The flow out of a nozzle determines dispensing and can be classified into a dripping and a jetting regime.[7] In the dripping case, a single droplet will form at the nozzle and detach under the gravitational pull once a critical volume is reached. The jetting regime is characterized by the persistence of a continuous jet for a certain length after the nozzle. The subsequent thinning and breaking of the liquid filament occurs on timescales larger than those of the fluid movement. For dispensing with a controlled volumetric flow, the free surface flow problem of the fluid exiting the orifice mainly determines these aspects. It is of particular interest how viscoelastic effects may slow down the filament breaking or affect the droplet size at pinch off. The breaking behavior will determine the minimum dispensable fluid volumes and the achievable dispensing frequencies.

However, the effects of viscoelastic and non-Newtonian fluid properties on dispensing are not yet fully understood. As stated by Li and Deng[7] in a recent review, ''the lack of mechanism research [is] the main reason why nearly all existing models are at best empirical formula.'' They furthermore specify that the ''… basic research for… fluid dispensing [that] is really lacking is [on]… the non-Newtonian properties of dispensing fluid materials and their influences on the dispensing process,… including shear thinning and extensional thickening [and the] influence on flow rate, fluid material breakup… and the whole dispensing process.''

The aim of this work is to map out the regimes where material property related problems with dispensing may occur. Specifically, we will present an operating space in terms of nondimensional groups. Within the operating space, we try to identify areas where dispensing could be problematic. To evaluate this experimentally, we have selected a number of model systems which represent the different classes of rheological behavior. The dispensing of these fluids has been monitored using high speed imaging. The article is structured as follows. The sections ''Materials'' and ''Experimental Methods'' introduce the different fluid classes, and how to experimentally determine their relevant material functions and parameters. The section ''Dimensional Analysis'' focuses on critical nondimensional parameters to classify the fluids and flow fields and introduces a 'map of misery' for the dispensing operations. The section ''Dispensing of Different Fluid Classes'' will then explore in detail the dispensing behavior of each fluid class with respect to the nondimensional parameters.

Additional Supporting Information may be found in the online version of this article.

Correspondence concerning this article should be addressed to C. Clasen at christian.clasen@cit.kuleuven.be.

Materials

Newtonian liquids

Four Newtonian liquids with viscosities covering four orders of magnitude have been used.

- PDMS 5: a low-viscosity polydimethylsiloxane (PDMS; Rhodorsil Oil 47V5, Bluestar Silicones, Lyon, France);
- PDMS 100: a medium-viscosity PDMS (Brookfield Viscosity Standard 98 mPas, Brookfield Engineering Laboratories, Middleboro, MA);
- PDMS 5000: a high-viscosity PDMS (Rhodorsil Oil 47V5000, Bluestar Silicones, Lyon, France);
- PIB: a very high-viscosity polyisobutylene (PIB) (Parapol 1300, Exxon Chemical, Houston, TX).

Shear thinning, inelastic power law liquid

As a model inelastic and shear thinning fluid, a suspension of rod-like virus particles was used. The semiflexible *fd* virus particles were grafted with a steric stabilizer, mPEG.[8] The particles were dispersed at a concentration of 7.78 wt % in a mixture of Tris buffer (5.22 wt %, pH 8.2, Trisma Base 99.9%, Sigma-Aldrich, Bornem, Belgium) and glycerol (87 wt %, BioUltra, Sigma-Aldrich, Bornem, Belgium).

Viscoelastic liquids

Three different viscoelastic solutions were prepared:

- PS in DEP: a medium-viscosity 2 wt % solution of polystyrene (PS) ($M_w = 3.84 \times 10^6$ g/mol, Polymer Laboratories, Amherst MA) in diethyl phthalate (DEP) (Merck, Darmstadt, Germany);
- PIB in Pristane: a high-viscosity 11 wt % solution of a PIB ($M_w = 1.2 \times 10^6$ g/mol, Sigma-Aldrich, Bornem, Belgium) in pristane (Sigma-Aldrich, Bornem, Belgium). This fluid is similar to the NIST Standard Reference Material (SRM 2490) that shows a characteristic viscoelastic behavior similar to that of polymeric melts with the advantage of being liquid at room temperature; [9]
- PIB in PIB (Boger Fluid): a solution of 0.2 wt % PIB ($M_w = 4.0 \times 10^6$ g/mol, Oppanol B200, BASF, Ludwigshafen, Germany) in a low-molecular weight PIB (Infineum S1054, Exxon Chemical, Houston, TX). This solution has the characteristics of a so-called "Boger fluid" with a nearly shear rate independent shear viscosity determined by the low-molecular weight PIB, but a high extensional viscosity and a long relaxation time caused by the high-molecular weight PIB fraction.

Experimental Methods

Volumetric controlled dispensing experiments were carried out with a PHD 4400 Hpsi syringe pump (Harvard Apparatus, Holliston, MA) and needle tips with inner/outer diameters of 0.84/1.27 and 1.54/1.83 mm (Nordson EFD, Westlake, OH), respectively. The dispensing was monitored with a high speed camera (FAST CAM SA2, Photron, San Diego, CA) and two different lenses: a telecentric objective with 55-mm focal length and adjustable magnification (TEC-M55 Computar, CBC, Tokyo, Japan), and a 50-mm f/1.2 objective (Nikkor, Nikon, Tokyo, Japan). Back light illumination was achieved with a fiber optic illuminator Fiber-Lite DC-950 (Dolan-Jenner Industries, Boxborough, MA).

The rheological properties of the fluids were measured with an ARES-G2 strain-controlled rotational rheometer (TA Instruments, Newcastle DE). The measurements were performed using a Couette geometry (cup diameter (mm)/bob diameter (mm): 34/32) and a cone and plate geometry (diameter 25 mm and angle 0.02 rad). The inelastic shear thinning system was characterized with a Physica MCR501 stress controlled rotational rheometer (Anton Paar GmbH, Graz, Austria) with a cone and plate geometry (diameter 25 mm and angle 2°). Flow curves are given in Figure 1. The viscosities η cover more than four orders of magnitude, and the behavior varies from Newtonian (PIB, PDMS 5, PDMS100, PDMS 5000) to strongly shear thinning (*fd*-suspension, PIB in pristane). The shear thinning can be characterized by a power law dependence on the second invariant of the rate of deformation tensor, II_{2D}, via a power law

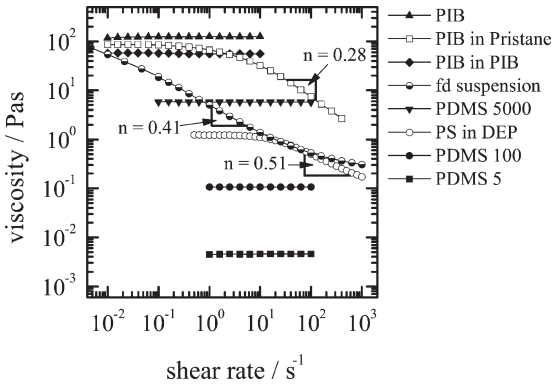

Figure 1. Flow curves.

Viscosity η as a function of the shear rate $\dot{\gamma}$ for the different model fluids.

$$\eta = K|II_{2D}|^{(n-1)/2} \quad (1)$$

where n is the power law exponent and K is the consistency index. For shear flow, the magnitude of the second invariant of the rate of deformation tensor equals $\dot{\gamma}^2$, with $\dot{\gamma}$ the shear rate. Apart from the non-Newtonian response, the viscoelastic nature is also of importance. To this end, the relaxation times λ were measured using a capillary breakup extensional rheometer (CaBER I, Thermo Fisher Scientific, Karlsruhe, Germany). This device applies a sudden stretch to a liquid drop via two round plates between which the drop is confined. The subsequent thinning of the liquid bridge under the action of surface tension was monitored with a laser micrometer. An exponential decay of the mid-filament radius was fitted with Eq. 25 to obtain the dominant relaxation time λ.[10]

The surface tension γ of the fluids was measured using a CAM 200 pendant drop apparatus (KSV Instruments Helsinki, Finland) and the fluid densities were obtained using a 10 cm^3 pycnometer (Brand Duran, Blaubrand, Germany). Material properties of all fluids are listed in Table 1.

Dimensional Analysis

Characteristic velocities

When a jet leaves a nozzle, there are several effects that contribute to the breakup. Surface tension will try to thin down the jet and cause droplets to pinch off. To this end, the velocity associated with capillary thinning must be fast enough compared to the velocity of the jet. The relevant thinning or the "capillary velocity" is given by the rate with which the radius of the jet, R, is decreasing as a function of time:

Table 1. Model Fluid Parameters

Fluid Units	ρ (kg/m$^{3)}$	γ (mN/m)	η_0 (Pa s)	K (Pa s^{2-n})	n	λ (s)
PDMS 5	911.2	18.6	0.0046	–	–	–
PDMS 100	966.0	20.2	0.106	–	–	–
PDMS 5000	974.4	20.5	5.81	–	–	–
PIB	901.3	30.9	123	–	–	–
PIB in pristane	793.7	24.9	88.0	200	0.28	0.057
PIB in PIB	891.2	31.5	58.4	–	–	26.4
PS in DEP	1118	37.5	1.03	4.75	0.51	0.023
fd suspension	1227	55.2	–	5.00	0.41	–

$$U = -\frac{dR}{dt} \tag{2}$$

The driving force of the filament thinning during dispensing originates from the capillary pressure and depends on, therefore, on the surface tension γ and the curvature ($1/R$) of the filament. Thus the capillary thinning is driven by γ, however, balanced by viscosity, fluid inertia, or elasticity depending on the fluid characteristics.

Viscosity Controlled Thinning. For a Newtonian liquid of sufficiently high viscosity, the capillary pressure γ/R is balanced by the viscous stress $\sigma = 3\eta\dot{\varepsilon}$, with the extension rate $\dot{\varepsilon} = -(2/R)(dR/dt)$. Assuming a cylindrical shape, this balance leads to a characteristic velocity $U = \gamma/(6\eta)$. A more detailed solution accounts for the nonuniform cylindrical shape. It has been shown that in the latter case the filament shape develops in a self-similar way, and one obtains a different numerical prefactor[11]

$$U_\eta = 0.0709\frac{\gamma}{\eta} \tag{3}$$

This viscosity controlled thinning velocity is constant and independent of the filament radius.

Inertia Controlled Thinning. For low-viscosity liquids, the dominant resistance against surface tension stems from the inertia of accelerating fluid elements.[12] In this case the characteristic capillary velocity depends on the density ρ as a material parameter and a characteristic velocity can be found from balancing the inertial and capillary stresses. Again, a quantitative description requires a solution of the filament shape which results in a numerical front factor[12–15]

$$U_\rho = 0.3413\sqrt{\frac{\gamma}{\rho R}} \tag{4}$$

The inertia controlled capillary velocity does depend on the filament radius R.

Elasticity Controlled Thinning. For viscoelastic fluids also elastic effects may oppose surface tension. For free surface flows of such an elasticity controlled viscoelastic fluid filament, the extension rate $\dot{\varepsilon}$ is constant and directly related to the inverse longest relaxation time λ of the liquid. The characteristic thinning velocity is given by balancing the elastic and capillary stresses

$$U_\lambda = \frac{1}{3}\frac{R}{\lambda} \tag{5}$$

where the numerical prefactor was determined by Entov and Hinch.[16] In this case, the characteristic velocity U_λ decreases linearly with the radius. It can be noted that for an elasticity controlled thinning U_λ is independent of the surface tension.

Comparing the characteristic velocities.

The filament thinning is determined by the balance of surface tension with the dominant resisting force. The latter depends on the relative magnitudes of the relevant fluid properties (η,ρ,λ). The lowest characteristic velocity of Eqs. 3–5 will determine the pathway from the initial diameter to the broken filament. Figure 2a provides the characteristic velocities for a low-viscosity viscoelastic fluid ($\eta = 0.033$ Pas, $\lambda = 0.0033$ s). In this case, as a function of time and changing filament radius, the thinning dynamics are successively controlled by inertia, viscosity, and elasticity. Figure 2 shows that the thinning mechanism can be expected to change as the filament radius decreases, depending on which material property provides the highest resistance against the squeezing of the surface tension, as indicated by the broken line in Figure 2a.

The evolution of the radius R with time can be obtained by integrating $U(t)$ and is given in Figure 2b for the low-viscosity viscoelastic fluid of Figure 2a. The time-dependent filament radius is indicated by the dashed line. Of course, it is too demanding a task to calculate these paths for each dispensing case. To determine which thinning mechanism is dominating at a certain filament diameter, nondimensional numbers provide a more practical approach. The nondimensional groups for free surface flows have been derived from the fundamental governing equations in the seminal work of

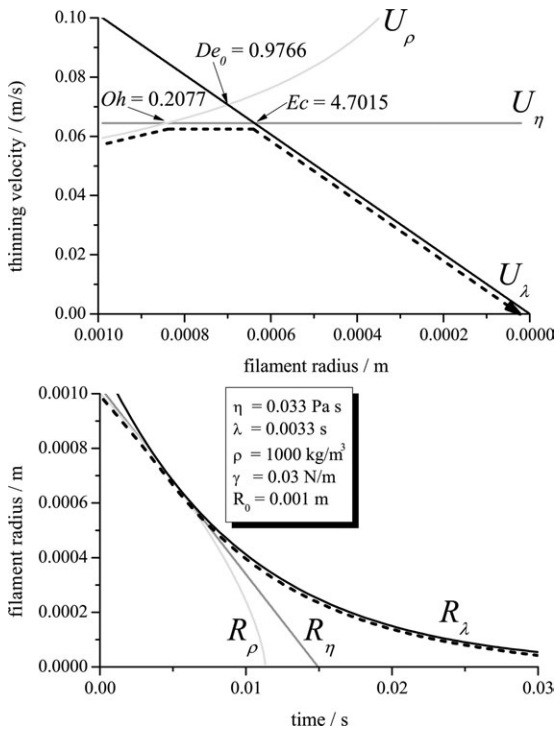

Figure 2. Example of complex thinning pathway.

(a) Theoretical filament thinning velocities $U = -dR/dt$ as a function of the filament radius R following Eqs. 3–5; (b) theoretical filament radius $R(t)$, following Eq. 17, 18, and 25. The dashed line in (a) indicates the lowest velocity for a given radius and, therefore, the actual radius evolution (dashed line in (b)) that the filament experiences during the thinning process.

Table 2. Material-Property-Based Nondimensional Numbers for Dispensing Using R_i, the Inner Nozzle Diameter

Fluid	R_i mm	Oh	De_0	Ec
PDMS 5	0.42	0.05	–	–
PDMS 100	0.42	1.18	–	–
PDMS 5000	0.42	63.3	–	–
PIB	0.77	839	–	–
PIB in pristane	0.77	704	15.1	0.02
PIB in PIB	0.77	397	7345	18.5
PS in DEP	1.18	4.63	3.30	0.705
fd virus	0.42	$\frac{U_\rho}{U_{\text{powerlaw}}} = 7.95$*	–	–

*Value refers to the equivalent Ohnesorge formulation of Eq. 23

Middleman.[17–20] These groups compare the characteristic velocities and identify three critical values. For reference, they will be reviewed here briefly.

The Ohnesorge Number Oh. The Ohnesorge number is typically defined for a slender filament and balances the viscous and inertial effects

$$Oh = \frac{\eta}{\sqrt{\rho\gamma R}} \tag{6}$$

For the case of nonuniform filament thinning and drop pinchoff, the numerical front factors of Eqs. 3 and 4 account for the finite curvature effects in axial direction. The critical Ohnesorge number at which the transition between viscosity and inertia dominated regimes takes place is indicated in Figure 2a. Its numerical value can be obtained by

$$\frac{U_\rho}{U_\eta} = \frac{Oh}{0.2077} \tag{7}$$

For Oh $>$ 0.2077 viscous effects will dominate the thinning and for $Oh < 0.2077$ the thinning will be controlled by inertia.

The Elasto-Capillary Number Ec. A similar comparison for the balance between the viscous and the elastic effects for an infinitely long fluid cylinder defines the elasto-capillary number as

$$Ec = \frac{\lambda\gamma}{\eta R} \tag{8}$$

Accounting for deviations from a slender body using Eqs 3 and 5, we obtain an expression for a critical elasto-capillary number as

$$\frac{U_\eta}{U_\lambda} = \frac{Ec}{4.7015} \tag{9}$$

Hence, viscosity controlled filament thinning dynamics are expected for $Ec < 4.7015$ and elastic effects for $Ec > 4.7015$. This critical Ec number is shown in Figure 2a.

The Intrinsic Deborah Number De_0. Balancing the elastic and inertial forces defines the so-called "intrinsic" Deborah number

$$De_0 = \sqrt{\frac{\lambda^2\gamma}{\rho R^3}} \tag{10}$$

This Deborah number (with the suffix 0) is denominated intrinsic or "natural," as it compares thinning velocities that are based solely on material properties and do not take the detailed geometry of the filament into account.[20] Accounting for axial curvature with Eqs. 4 and 5, the transition criterion becomes

$$\frac{U_\rho}{U_\lambda} = \frac{De_0}{0.9766} \tag{11}$$

One additional group that governs the dynamics for large nozzle radii is the gravitational Bond number $\rho g R^2/\gamma$. However, this group does not vary if the nozzle radius is held fixed.

It should be noted that only two out of the three dimensionless groups Oh, De, and Ec are independent and that $De/Ec = Oh$. Furthermore, when using these nondimensional numbers, it should be noted that they can be determined in two different ways. If the characteristic length scale that enters the number is taken to be the initial filament diameter R_0, one obtains overall or "global" nondimensional numbers. This is often done to make an initial estimation of the overall thinning dynamics.[20] Conversely, one can calculate a "local" number to determine at what radius a transition from one thinning regime to the other is to be expected, as was done in Figure 2a. In this case, the radius that enters the nondimensional number is $R(t)$. Often, the equation is inverted to calculate the radius $R(t)$ at which the critical nondimensional number is reached. For the fluids studied in this work, the global nondimensional numbers are given in Table 2. It can be seen that the range of nondimensional groups should enable us to explore a range of breakup pathways.

The "map of misery": the operating space for dispensing

The nondimensional groups Oh, De_0, and Ec compare the magnitudes of the thinning velocities for a given filament radius. Oh, De_0, and Ec depend only on material parameters and the filament radius which is determined by the radius of the nozzle of the dispenser. The parameter space that they are spanning (Figure 3) fully defines, for a given initial radius R_0, which material property dominates the thinning behavior at the beginning of the breaking process. For example, for the PIB in pristane solution Table 2 teaches us that

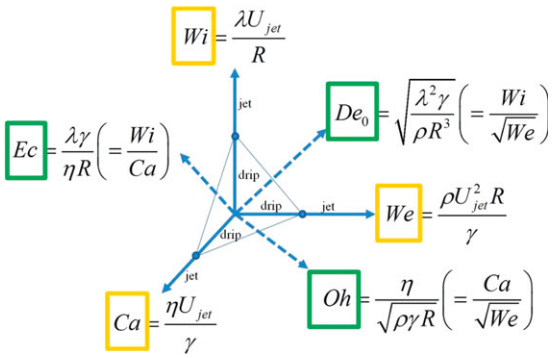

Figure 3. Operating space for dispensing.

Material-property-based nondimensional Ohnesorge number *Oh*, elasto-capillary number *Ec* and intrinsic Deborah number De_0. The respective dynamic nondimensional Weber number *We*, capillary number *Ca*, and Weissenberg number *Wi* indicate the transition between a dripping and a jetting dispensing for the respective dominating material property (inertia, viscosity, or elasticity) as described by *Oh*, *Ec* and De_0. [Color figure can be viewed in the online issue, which is available at wileyonlinelibrary.com.]

not only $Oh = 704 \gg 0.2$, indicating that viscosity is more important than inertia, but also $De_0 = 15.1 > 1$, so that also elasticity will dominate over inertia. Ec can be used to assess if viscosity or elasticity is providing more resistance, and with $Ec = 0.02 \ll 4.7$ it is obvious that a filament thinning will initially be controlled by viscosity as the dominating material parameter.

The material parameters and the associated nondimensional numbers, thus, allow one to identify the initial thinning mechanism. Once this is established, the relevant thinning velocity has to be compared to the velocity of the jet U_{jet} to identify if one will be in the dripping or in the jetting regime. To compare the time needed for the jet to breakup vs the characteristic time associated with the convective jetting velocity (which is taken as the time for the jet to travel a distance equal to R_0), another set of dynamic nondimensional groups can be defined. Only if the travel time of a fluid element over a distance R_0 is shorter than the breaking time, the breaking point will be convected away and a jet is formed. When viscous thinning is the dominant mechanism the relevant dynamic nondimensional number that compares U_η with U_{jet} is the capillary number, defined as

$$Ca = \frac{\eta_0 U_{\text{jet}}}{\gamma} \tag{12}$$

When inertial dynamics dominate the thinning the Weber number compares U_ρ with U_{jet} and is defined as

$$We = \frac{\rho U_{\text{jet}}^2 R}{\gamma} \tag{13}$$

Finally, for elastic fluids the relevant dynamic nondimensional group (comparing U_λ with U_{jet}) is given by the Weissenberg number

$$Wi = \frac{\lambda U_{\text{jet}}}{R} \tag{14}$$

For each of these dynamic nondimensional groups, a critical *Ca, We*, or *Wi* can be identified which defines the transition from a dripping to a jetting state. The case of the capillary number is the most simple one. As U_η is constant, Ca is independent of the initial radius R_0. The critical Weber number depends on the filament radius. The radius also enters the Weissenberg number, however, in this case the elastic velocity U_λ (Eq. 5) is going to 0 for decreasing filament diameters and an ideal elastic filament would never break. In reality, finite extensibility of the elastic components will lead to a breaking of the filament. An additional parameter will then be required (not pursued here) to describe the transition from dripping to jetting.

Figure 3 represents a diagram of the operating space for steady-state dispensing, in terms of the material-property-based nondimensional groups *Oh, De*$_0$, and *Ec*. The dynamic numbers *Ca, We*, and *Wi* define paths within this operating space. The knowledge of *Oh, De*$_0$, and *Ec* allows one to determine the controlling material property and sets the appropriate dynamic number to calculate the dripping/jetting transition. It should be noted that the six nondimensional groups are interrelated. As it is also shown in Figure 3, the Ohnesorge number can be calculated from $Oh = Ca/\sqrt{We}$, and similarly $Ec = Wi/Ca$ and $De_0 = Wi/\sqrt{We}$. With this it is obvious that a dispensing operation is fully described by any set of two material-property-based and one dynamic nondimensional groups. The remaining three groups can then be calculated (for example for known *Oh*, *De*, and *We* one obtains $Ca = Oh\sqrt{We}$, $Wi = De\sqrt{We}$, and $Ec = De/Oh$).

One problem that can arise when using global nondimensional numbers is the assumption that the initially dominating material property will continue to determine the thinning mechanism until the filament is finally broken. However, we will often encounter a situation where the initial radius leads to a global nondimensional number close to a critical transition. The time-dependent filament radius $R(t)$ may then lead to a critical local nondimensional number and a transition to thinning dynamics different from the global number, as was, for example, shown in Figure 2. Viscoelastic fluids in particular can reach very large breakup times in the elastically controlled thinning. For example, the calculation of the global numbers might indicate that $Ec < 4.7015$, even though the overall breaking behavior will be dominated by the elastic thinning. Close to the critical values of *Ec* or De_0, plotting the velocity vs. radius curves as done in Figure 2a is then more useful and allows one to identify which material parameters need to be tuned to achieve a desired dispensing behavior.

Dispensing of Different Fluid Classes

The dispensing accuracy of a liquid is related to the flow rate and the precision of the time interval required to achieve steady-state flow, or to stop the flow.[21] A discussion of the mechanical elements of the flow control is beyond the scope of this article. In this work, we will focus on the problems in volumetric flow controlled dispensing that may arise from the intrinsic nature of the fluid.

Inertia controlled regime

Drop Dimensions. When the flow rate is low enough, the liquid will be in the dripping regime. A droplet will form under the action of the surface tension, fed by the fluid influx until the mass is large enough for gravitational forces to overcome the capillary forces, as shown in Figure 4a. An individual droplet will form, and the volume V_{drip} of the droplet determines the precision of dispensing at low-flow rates. It can be described by the Harkins-Brown relation[22,23]

$$V_{\text{drip}} = f_{\text{HB}} \frac{2\pi\gamma R}{\rho g} \tag{15}$$

where γ is the surface tension, ρ is the density of the liquid, and R is the radius of the orifice. Note that for the case of a nonwetting material the inner radius R_{i} of the nozzle orifice should be used and for a wetting material the outer radius R_{e}.[24] The coefficient f_{HB} accounts for the nonsphericity due to gravity and is a function of the ratio $\gamma/\rho g$ and the radius R. A recent calculation by Yildirim et al.[25] has shown that $f_{\text{HB}} \simeq 0.6248\, R^{-0.1352}(\gamma/\rho g)^{0.0676}$ which is valid over a wide range of $0 < R/V_{\text{drip}}^{1/3} < 1.0$. For low-viscosity fluids the Harkins–Brown relation Eq. 15 is independent of the feeding flow rate for low flow rates ($We < 10^{-5}$).[25]

One thing to note is that the dispensing of a low-viscosity solution in the inertia controlled regime always involves the formation of a much smaller satellite droplet[26] as can be seen in the last four frames of Figure 4a. As the trajectories

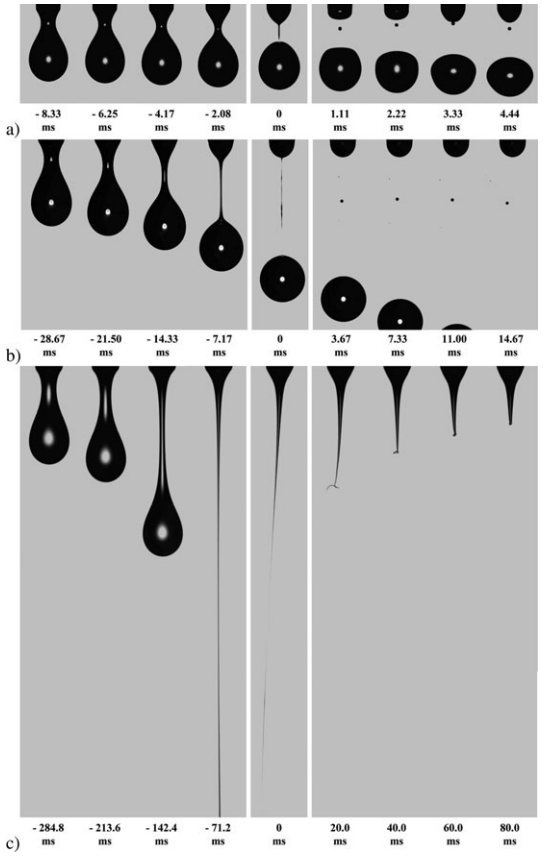

Figure 4. Dispensing of Newtonian fluids of different viscosity.

(a) PDMS 5, (b) PDMS 100, and (c) PDMS 5000 from a nozzle with inner radius $R_i = 0.42$ mm (the time to the breaking event is given below each frame). The relevant nondimensional numbers calculate to (a) $Oh = 0.05$, (b) $Oh = 1.18$ and (c) $Oh = 63.3$, corresponding to (a) an inertia and for (b) and (c) a viscosity-controlled dispensing. The dispensing is for (a) with a Weber number of $We = 0.0005$ and for (b) and (c) with capillary numbers of $Ca = 0.02$ and $Ca = 0.14$ in all three cases in the dripping regime.

of these satellite droplets do not necessarily follow that of the large leading drop, the satellite can lead to spilling and "misting" or a general unclean dispensing and inaccurate amounts of the dispensed fluid for $Oh < 1$.

Dripping/Jetting Transition. At high-flow rates, the liquid is jetting out of the dispensing nozzle, and the breakup event is convected away from the orifice. A dispensing in jetting mode allows a higher precision compared with the dripping mode as it is not discrete. The jet can be disrupted at any given moment at the orifice by stopping the flow, allowing a continuous adjustment of the dispensed volume now only depending on the mechanical precision of the flow control. The transition between dripping and jetting in an inertia controlled thinning is determined by a range of Weber numbers. A first transition, from regular dripping to chaotic dripping, is taking place at Weber numbers on the order of $We = O(0.1)$.[27] When further increasing the flow rate, a second transition at $We = O(1)$ is observed where a sudden shift of the breaking point away from the orifice occurs. For small nozzle diameter, the critical Weber number at the second transition approaches a constant value of $We_c \sim 2$ [27]. The dispensing of the PDMS 5 fluid in Figure 4a (of which a movie can be seen in the Supporting Information 'PDMS 5 - We = 0.0005.avi') is with $We = 0.0005$ still in the regular dripping regime. At $We = 2.53$ the dispensing of PDMS 5 is in the jetting regime as it can be seen in the movie in the Supporting Information 'PDMS 5 - We = 2.53.avi'.

Filament Lifetime. The time that it takes for an inertia controlled filament to break, is given by

$$t_c = \int_R^0 \frac{dR}{U_\rho} = 1.9531\sqrt{\frac{\rho R_0^3}{\gamma}} \tag{16}$$

with the radius of the filament evolving with time t following[12,15,28]

$$R = 0.64\left(\frac{\gamma}{\rho}\right)^{\frac{1}{3}}(t_c - t)^{\frac{2}{3}} \tag{17}$$

For the dripping case, the radius of the liquid bridge holding the pendant droplet when the thinning sets in is slightly smaller than R_0. However, the time that it takes for the filament to break once another critical volume V_{drip} is dispensed can readily be estimated with R_0. For example, calculating the breaking time with Eq. 16 for the inertia controlled model fluid PDMS 5 dispensed in Figure 4a gives $t_c = 3.7$ ms. This value is in good agreement with the experimentally observed 4.2 ms to breakup (third frame of Figure 4a).

Viscous regime

Filament Lifetime. The filament lifetime increases with viscosity. Above the critical Ohnesorge number of Eq. 7 the filament thins and breaks in the middle between the droplets controlled by viscosity.[29] An example is shown in the fourth frame of Figures 4b,c. In this case, a constant thinning velocity (Eq. 3) is observed. The radius of this viscous filament decays linear in time as

$$R = R_0 - 0.0709\frac{\gamma}{\eta}t \tag{18}$$

This is shown in Figure 2 where R in the viscosity dominated regime is indicated as R_η. The numerical front factor originates from the self-similarity in the shape of the filament as determined by Papageorgiou[11,30] and Pozrikidis.[31] The time to breakup of the filament t_c is then

$$t_c = 14.1\eta R_0/\gamma \tag{19}$$

For example, for the PDMS 100 fluid dispensed in Figure 4b with a viscosity of $\eta = 0.1$ Pas we predict a breaking time on the order of $t_c = 31$ ms which is in good agreement with the experimentally observed breaking time 29 ms in Figure 4b.

At higher viscosities, an additional phenomenon is further complicating the dispensing of a Newtonian liquid. The large mass of fluid (accumulated due to the slow breaking dynamics) will exert a gravitational pull on the filament connected to the nozzle. For a dripping dispensing this causes an additional stretching that can accelerate the thinning, and this is observed for example, for the high-viscosity PIB fluid ($Oh = 839$) in Figure 5, where the breaking event is clearly faster than the calculated breaking time of $t_c = 43$ s via Eq. 19. However, for a jetting dispensing this "gravitational stretching" of the viscous filament hinders the development of the necking instability and delays the breaking time. This effect

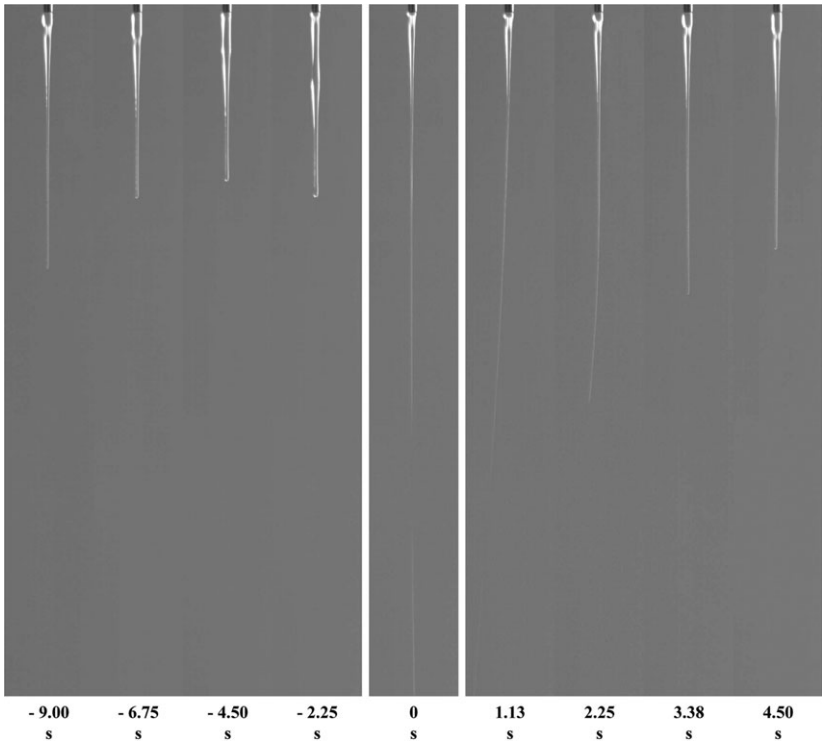

Figure 5. Drop dimensions in a viscous Newtonian fluid.

Dispensing of a high-viscosity Newtonian PIB fluid from a nozzle with inner radius $R_i = 0.77$ mm (the time to the breaking event is given in seconds) with $Oh = 839$. The dispensing is with a dynamic nondimensional capillary number of $Ca = 5.9$ close to the jetting transition, but still in the dripping regime.

is still under investigation.[32,33] It can be noted that dispensing of such highly viscous liquids through a nozzle is seldom performed due to the very long dispensing times and energy requirements.

A note on the side: Eggers[28,34,35] determined an asymmetric similarity solution for the thinning filament that gives a smaller front factor of 0.0304 compared to that of 0.0709 in Eqs. 18 and 3

$$R = R_0 - 0.0304\frac{\gamma}{\mu}t. \tag{20}$$

This similarity solution applies when velocities in the filament become so large that inertia can no longer be neglected. However, Eq. 20 does not contain the density and the main role of inertia is in the development of an asymmetric shape of the thinning filament. This causes a vertical shift of the necking point along the filament towards the drop when approaching the breaking point. The transition from a viscosity controlled thinning to this Eggers scaling regime is in theory reported to take place at a radius of $R = R_0 Oh^{2/(2\beta-1)} \sim 1$ (with the global $Oh = \eta/\sqrt{\rho\gamma R_0}$ and $\beta = 0.17487$).[4,32,36] However, there is a large discrepancy to experimental data that is at present not yet understood and the observed transition takes place at radii an order of magnitude smaller than the theoretical value.[32,37,38] Eventually, also low-viscosity fluids that initially follow Eq. 17 will switch over to the Eggers solution, a qualitative transition criterion for this case is discussed to be a local Ohnesorge number of $Oh^2 \sim 1$.[4,13,39,40] In all the cases, the transition to the Eggers thinning takes place at very small filament radii so that the effect on a dispensing operation is negligible.

Dripping/Jetting Transition. For $Oh > 0.2$, the relevant dynamic number is the capillary number Ca. The dispensing of the PDMS 5000 fluid in Figure 4c (of which a movie can be seen in the Supporting Information 'PDMS 5000 - $Ca = 0.14$.avi') is with $Ca = 0.14$ still in the dripping regime. At $Ca = 8.5$ the dispensing is in the jetting regime (as it can be seen in the movie in the Supporting Information, 'PDMS 5000 - $Ca = 8.5$.avi'). A detailed investigation of the dripping/jetting transition has shown that the critical capillary number for all needle diameters used in this study is reached at $Ca \sim 6.5$. It should be noted that for high-viscosity fluids the exact value for a transition is more difficult to observe due to the gravitational stretching. Furthermore, the longer times necessary for the onset of thinning and the final breaking times lead to long breaking distances already at the transition.

Approaching the critical Ohnesorge number suppresses the chaotic dripping regime observed for low-viscosity systems. Above a Ohnesorge number of $Oh = 0.8$ a smooth transition from regular dripping to jetting is observed.[41]

Drop Dimensions. For viscous fluids with $Oh > 0.2$, the volume of the drop is described by the Harkins–Brown relation, Eq. 15, for low enough flow rates.[25] However, as can be seen in Figure 5 for the high-viscosity PIB ($Oh = 839$), the drop will not necessarily take on a spherical shape. Moreover, increasing the Ohnesorge number above the critical value of $Oh = 0.2$ reduces satellite droplet sizes [42,43] up to the point where they are suppressed.[44,45] The inertia controlled pinching of the filament close to the end drops is no longer observed. Instead, the viscosity controlled breaking of the filament in the middle between the droplets and the surface tension driven retraction of the stumps into the drops

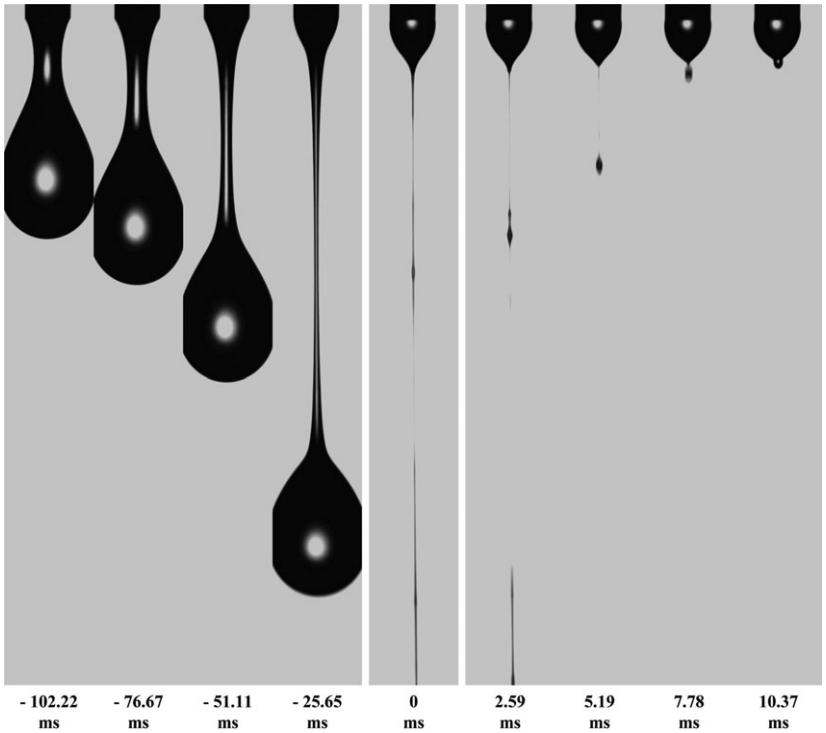

Figure 6. Dispensing of a shear thinning *fd* virus suspension at $Oh = U_\rho/U_{\text{powerlaw}} = 7.9$ ($R_i = 0.42$ mm, and the time to the breaking event is given in ms).

A movie of this sequence can be seen in the Supporting Information 'fd virus — *Ca*-powerlaw = 0.37.avi'.

prevents the formation of satellite drops (see e.g., PDMS 5000 ($Oh = 63.3$) in Figure 4c and the PIB fluid ($Oh = 839$) in Figure 5). The dispensing of the PDMS 100 fluid with $Oh = 1.18$ in Figure 4b still leads to a satellite drop formation as this fluid is still close to the critical Ohnesorge value. For a satellite-free dispensing, Oh needs to be $\gg 1$.

Power law fluids

Fluids that are not elastic, and for which the viscosity η is a function of the deformation rate and decreases with increasing rate, are called power law fluids as defined by Eq. 1. The second invariant of the rate of deformation tensor II_{2D} is for the extensional flow encountered in the filament $II_{2D} = -3\dot{\varepsilon}^2$, so that for the dispensing of a power law fluid $\eta = 3^{(n-1)/2}K\dot{\varepsilon}^{n-1}$ and the fluid shows also an extension thinning. When Oh is sufficiently large, the deformation thinning will influence filament breaking dynamics. The decrease in viscosity at the necking point between two droplets will cause a positive feedback and lead to a continuous acceleration of the necking. This leads to a faster breaking compared to a Newtonian liquid of similar initial viscosity, as seen for the shear thinning *fd* suspension in Figure 6. Although Figure 1 shows that the initial low shear rate value of the viscosity is similar to the PIB fluid in Figure 5, the power law dependence of the viscosity of the *fd* suspension leads to a breakup time in Figure 6 that is two orders of magnitude smaller than for the PIB fluid.

Filament Lifetime. The time necessary for the jet to break up into single droplets can be calculated once the power law parameters are known. The parameters n and K can be extracted from the shear flow experiments in Figure 1 for which $II_{2D} = \dot{\gamma}^2$ and $\eta = K\dot{\gamma}^{n-1}$. The jet radius at a necking point between two drops evolves with time t following[38]

$$R = \Phi\frac{\gamma}{K}(t_c - t)^n \tag{21}$$

where the prefactor Φ depends on the power law exponent n (values for Φ are given in Table 3).[38,20] The breakup time is then $t_c = (R_0K/\Phi\sigma)^{(1/n)}$.

A consequence of the faster than Newtonian breaking is that the critical velocity for a transition from dripping to jetting shifts to higher values. The capillary velocity of a power law fluid can be obtained by differentiating Eq. 21

$$U_{\text{powerlaw}} = n\Phi^{\frac{1}{n}}\left(\frac{\gamma}{K}\right)^{\frac{1}{n}}R^{\left(1-\frac{1}{n}\right)} \tag{22}$$

and the generalized nondimensional numbers can be obtained. The inertia controlled capillary velocity from Eq. 4 divided by U_{powerlaw} gives a transition criterion similar to the Ohnesorge number definition of Eq. 7

$$\frac{U_\rho}{U_{\text{powerlaw}}} = \frac{0.3413}{n\Phi^{\frac{1}{n}}}\frac{K^{\frac{1}{n}}}{\rho^{\frac{1}{2}}\gamma^{\left(\frac{1}{n}-\frac{1}{2}\right)}R^{\left(\frac{3}{2}-\frac{1}{n}\right)}} \tag{23}$$

This equation reduces to Eq. 7 for Newtonian fluids with $n = 1$. For weakly deformation thinning fluids with $2/3 < n < 1$, the transition from inertia to viscosity controlled filament thinning is delayed. For a power law index of $n = 2/3$, the ratio of the inertial and viscous velocities becomes independent of the radius R. In this case, the velocity $U_{\text{powerlaw}} \sim R^{-0.5}$ depends on the radius with the same power as the inertial velocity U_ρ in Eq. 4 and these two velocity vs radius curves will never cross. In this case, only the other variables K, γ, and ρ determine if the filament thinning behavior is determined by viscosity or inertia. For fluids with $0 < n <$

Table 3. Prefactor Φ for a Power Law Fluid for Different Power Law Exponents n[38,46]

n	Φ
1.0	0.0709
0.9	0.101
0.8	0.143
0.7	0.200
0.6	0.260
0.5	0.259
0.4	0.228

2/3, the acceleration of the filament thinning rate U_{powerlaw} is faster than for U_ρ. This means that at the critical radius condition in Eq. 23 (when $U_{\text{powerlaw}} = U_{\text{q}}$) the thinning dynamics switch from a viscosity controlled filament thinning back to an inertia controlled thinning with a decreasing filament radius following Eq. 17. The dispensing of a power law fluid with $n = 0.41$ (obtained from Figure 1) is shown in Figure 6. Because of the relatively high viscosity of this fluid ($K = 5$ in Eq. 23) the critical radius is of order $O(10\mu\text{m})$ and inertia affects the breaking only at the final stage (frame five in Figure 6). Numerical simulations[4] have identified conditions for the inertia controlled thinning for $n < 2/3$.

Dripping/Jetting Transition. For viscosity controlled thinning, the transition from dripping to jetting can be calculated via a comparison of velocities similar to the capillary number Ca definition of Eq. 12

$$Ca_{\text{powerlaw}} = \frac{U_{\text{jet}}}{U_{\text{powerlaw}}} = \frac{1}{n}\Phi^{-\frac{1}{n}}\frac{K^{\frac{1}{n}}U_{\text{jet}}}{\gamma^{\frac{1}{n}}R^{\left(1-\frac{1}{n}\right)}} \tag{24}$$

Although there are no experiments on the dripping/jetting transition for power law fluids reported, numerical simulations indicate that the velocity for the dripping/jetting transition doubles[46] compared to the Newtonian case. Exact criteria for a critical value of Ca_{powerlaw} of Eq. 24 are not yet established, but expected to be on the same order as for the Newtonian case in section "Dripping/Jetting Transition." The dispensing in Figure 6 (of which a movie can be seen in the Supporting Information, 'fd virus - Ca-powerlaw = 0.37.avi') is with $Ca_{\text{powerlaw}} = 0.37$ still in the dripping regime. At $Ca_{\text{powerlaw}} = 25.8$, the dispensing is already in the jetting regime (see movie in the Supporting Information, 'fd virus - Ca-powerlaw = 25.8.avi').

Drop Dimensions. The drop volume for both jetting and dripping dispensing are similar to the Newtonian case. However, the criteria for a satellite droplet formation are different for a power law fluid. As shown by Suryo and Basaran,[4] the critical value of $Oh = 0.2$ is not valid for power law fluids. Power law fluids will, even for an initial viscosity controlled thinning, finally break following an inertia control with satellite droplet formation due to the decreasing viscosity during the filament thinning process. The example in Figure 6 shows, from frame 4 onward, the development of a satellite drop on the filament that is, however, consumed by the pendant droplet.

Viscoelastic fluids

Viscoelastic fluids, such as polymers in melt or in solution, are generally more difficult to dispense than Newtonian or power law fluids. Although they are often shear thinning, they behave differently in extensional flows. Depending on the base viscosity of the fluid, we can generally formulate two different classes of viscoelastic fluids for dispensing operations:

1. The first class are liquids with high viscosity levels and $Oh \gg 0.2$. In this case it is the elasto-capillary number Ec that determines if the fluid is weakly elastic (for $Ec \ll 4.7$) and will behave like a viscous Newtonian fluid or a power law fluid as discussed in sections "Viscous regime" and "Power law fluids," or if it will be dominated by an elastic response (for $Ec \gg 4.7$).

2. The second class is for $Oh \ll 0.2$ and, therefore, low-viscosity or inviscid solutions. As we can see from Figure 3 it is in this case the intrinsic Deborah number De_0 that determines if the fluid is only weakly elastic (for $De_0 \ll 1$) and behaves, therefore, as a low-viscosity Newtonian liquid as discussed in section "Inertia controlled regime", or if it behaves inviscid but elastic (for $De_0 \gg 1$).

Viscoelastic liquids with a high viscosity

Weakly Elastic Liquids with Oh $\gg$ *0.2 and* Ec $\ll$ *4.7.* For viscoelastic liquids with a high viscosity ($Oh \gg 0.2$), but a weak elastic response such that $Ec \ll 4.7$, the viscosity is dominant. The dispensing is initially faster compared with that of a purely Newtonian liquid of similar viscosity level because of the time-dependent development of elastic stresses.[26] The reason why many semidilute and concentrated polymer solutions have $Ec \ll 4.7$ and exhibit a weakly elastic behavior,[47,48] is that the relaxation time of the fluid λ that enters Eq. 8 is the Rouse time for molecular stretching rather than the longest relaxation time of reptation of the polymer.[47,49] While this relaxation time increases with increasing polymer concentration, the ratio λ/η that enters the elasto-capillary number is decreasing due to the high viscosity η of entangled polymer solutions.[48] In spite of a lack of a quantitative theory, these weakly elastic fluids with a low ratio λ/η are "uncomplicated" in dispensing operations as they follow the simple Newtonian or an even faster power law thinning. The breakup times and the dripping/jetting transition can be calculated using the analysis of section "Viscous regime" and "Power law fluids."

One example of this class of fluids is given in Figure 7. Although the PIB in pristane solution has a relaxation time λ of 57 ms and would be generally considered as a strongly "viscoelastic" solution, the calculated elasto-capillary number is $Ec = 0.02$, which indicates that for a dispensing operation this fluid will behave only weakly elastic. Indeed, comparing the qualitative dispensing behavior in Figure 7 and 5, the PIB in pristane fluid behaves as the Newtonian PIB fluid of similar zero-shear viscosity. A theoretical breaking time of $t_c = 15$ s calculated from Eq. 19 for a Newtonian liquid gives a good order of magnitude estimate of the observed dispensing time of ~ 7 s observed in Figure 7.

Elastic Liquids with Oh $\gg$ *0.2 and* Ec $>$ *4.7.* Viscoelastic solutions of high viscosity and with $Ec > 4.7$ represent one of the most difficult fluid classes for dispensing. In these elastic solutions, the nonlinear elastic stresses will rapidly develop in the thinning filament and will slow the breaking dynamics dramatically. For polymeric fluids this behavior is observed in dilute and semidilute solutions with a low number of entanglements.[50] In particular, when it is possible to increase the relaxation time λ without significantly affecting the viscosity η high elasto-capillary numbers are possible. This is encountered for surfactant solutions that

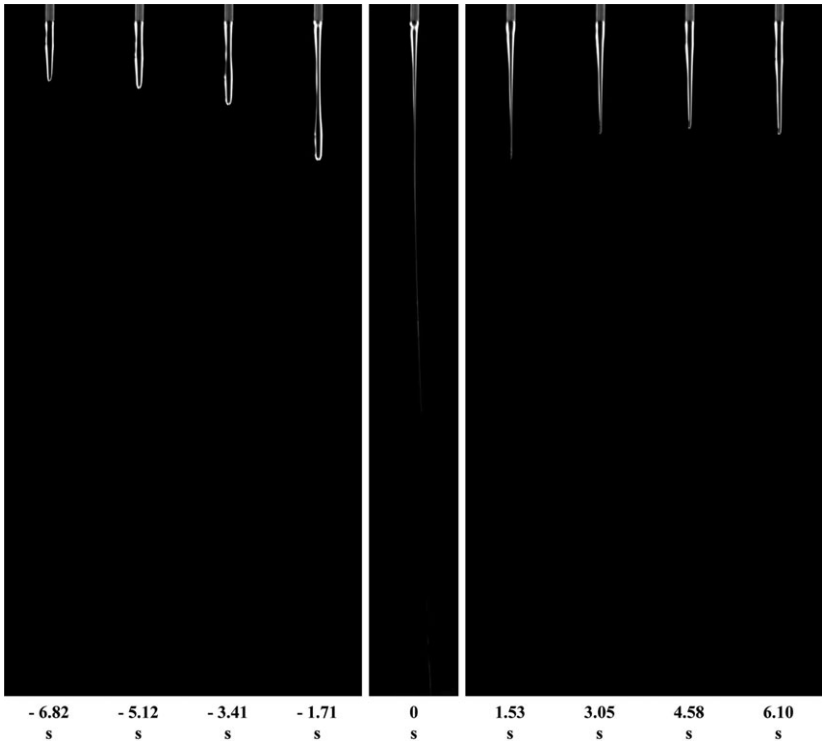

Figure 7. Dispensing of a viscous, weakly elastic solution.

Viscosity-controlled dispensing of PIB in pristane with $Oh = 703$, $Ec = 0.02$ and $De = 15.1$ ($R_i = 0.77$ mm, the time to the breaking event is given in seconds). The dispensing is in the dripping regime with $Ca = 5.12$.

form worm-like micelles,[51] dilute polymer solutions, and in the so-called Boger fluids. [52,53] For a Boger fluid, λ can be raised by increasing the molecular weight of a polymer dissolved at low concentrations in a high-viscosity solvent with only small changes in the viscosity η. This enables achieving elasto-capillary numbers Ec way above the critical value of $Ec = 4.7$ given in Eq. 9. In addition to this, in Boger fluids the relaxation time is proportional to the viscosity, $\lambda \sim \eta$. Thus, increasing the (solvent) viscosity will not change Ec, but it will lead to even longer relaxation times and, therefore, to longer breakup times and a more difficult dispensing. An example of the dispensing of such a Boger fluid is given with the PIB in PIB fluid in Figure 8. Although this fluid has a viscosity of the same order of magnitude as the weakly elastic fluid in Figure 7, it has a breaking time two orders of magnitude larger, and indeed with $Ec = 18.5$ the thinning is indicated to be controlled by elasticity.

Filament Lifetime. The most prominent effect observed for an elastically dominated fluid is the increase in breakup time. Although the droplet volume is the same as for the dripping of a Newtonian liquid,[46] a viscoelastic solution can show very long living filaments that connect the drop to the nozzle and that can cause spillage. As already pointed out in section "Dimensional Analysis" the time dependence of viscoelastic effects "softens" the hard numerical values for the critical elasticity number $Ec = 4.7$ or intrinsic Deborah number $De_0 = 1$. A quantitative description needs to take into account five different stages of filament thinning.[48] However, even a full knowledge of fluid parameters does not allow a quantitative prediction of the breaking time. The important point here is that whenever the "map of misery" of Figure 3 indicates that $Ec > 4.7$ (and $Oh \gg 0.2$) strong viscoelastic effects can cause problems in dispensing operations.

The different regimes (I–V) that govern the thinning of a filament can be exemplary identified for a solution of PS in DEP in the plots of $R(t)$ and $U(t)$ as shown in Figures 9 and 10.

(I) In the first regime, elastic stresses arising from flow in the dispensing nozzle can stabilize the liquid filament right after exiting the nozzle. The contraction flow leads to a prestrech, which will stabilize the jet and delay the onset of the instability leading to breakup.[26] A similar prestretch occurs at the nozzle exit, where fluid elements stuck to the nozzle wall are accelerated to the average velocity of the jet.[3,54] The capillary breakup experiment in Figure 9 does not fully reproduce the prestretch and hence, only has a limited stabilization.[55]

(II) In the second regime, the thinning velocity $U_\eta(t)$ of the filament is constant (Eq. 3). The radius follows the thinning $R_\eta(t)$ for a viscosity-dominated regime (Eq. 18). This linear thinning regime II is clearly observed in the radius (Figure 9) as well as the velocity (Figure 10) of the PS in DEP solution. For a weakly elastic solution, regime II will be most dominantly present. An example is given in Figure 11 that shows the filament radius evolution for the PIB in pristane that was dispensed in Figure 7.

(III) The third regime shows an increasing thinning velocity due to a decreasing viscosity in the extensional flow field[26,56,57] similar to the thinning of a power law fluid. The velocity and filament profile evolution follow Eq. 22 and 21, respectively. Figure 9 shows regime III for PS in DEP, and for the weakly elastic PIB in pristane regime III is visible in the inset of Figure 11.

(IV) In the fourth regime, the elastic effects of the fluid dominate. A strain hardening of the extensional viscosity causes slower breakup dynamics compared to Newtonian fluids of comparable shear viscosities. In this regime, the filament thins exponentially with time[10,16]

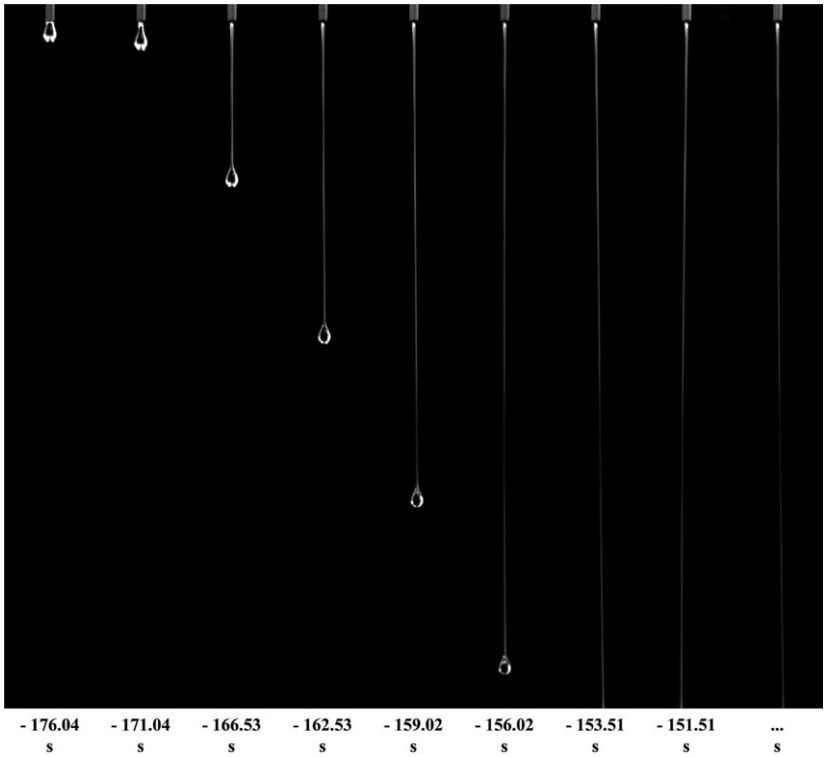

Figure 8. Dispensing of a Boger Fluid.

Elastic controlled dispensing of PIB in PIB at $Oh = 397$, $Ec = 18.5$, and $De = 7345$ ($R_i = 0.77$ mm). Filament breaking time is $t_c = 176$ S (only frames for the first 25 s are shown). A movie of this sequence can be seen in the Supporting Information 'PIB in PIB - Wi = 5.11.avi'.

$$R_\lambda \sim \exp\left(\frac{-t}{3\lambda}\right) \tag{25}$$

which agrees well with the observed regime IV in Figure 9. The onset of this fourth, elastic thinning regime can depend on the deformation history of the filament. For the relatively low elasto-capillary number of $Ec = 0.71$ in Figures 9 and 10, the onset of this regime IV is observed only after the initial filament radius has decreased by an order of magnitude. However, whenever regime IV can set in, the breakup time is greatly increased.

(V) In the quasilinear limit of infinite extensibility, regime IV would continue, but in reality the polymers reach their finite extensibility limits and the filament thins faster toward the final breakup and separation of the drops (as indicated for the elastic PS in DEP solution in the semilog inset in Figure 9). Again, the onset of this regime depends on the

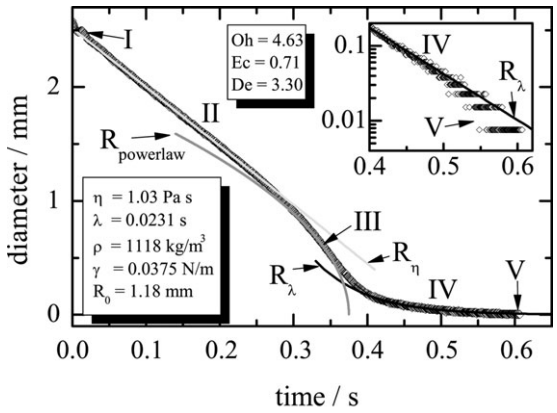

Figure 9. Evolution of the filament radius for an elastic fluid.

A viscoelastic solution of PS in DEP (open symbols) is compared to the predictions for a Newtonian fluid ($R_\eta(t)$, Eq. 18), a power law fluid ($R_{powerlaw}(t)$, Eq. 21), and an elasticity controlled fluid ($R_\lambda(t)$, Eq. 25). The different thinning regimes for viscoelastic solutions as discussed in the text are indicated with roman numeral I–V. The inset highlights on a logarithmic scale the onset of the finite extensibility limit in regime V.

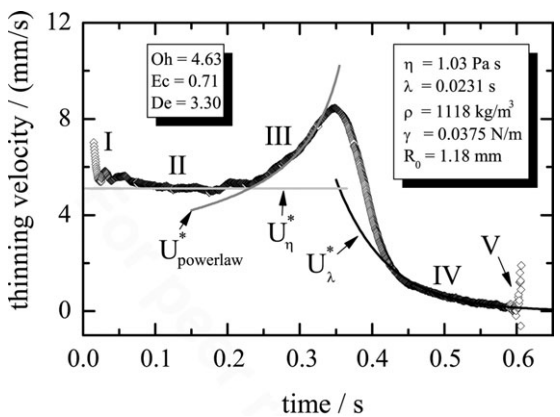

Figure 10. Evolution of the thinning velocity for an elastic fluid.

A viscoelastic solution of PS in DEP (open symbols) is compared to the predictions for a Newtonian fluid ($U_\eta(t)$, Eq. 3), a power law fluid ($U_{powerlaw}(t)$, Eq. 22), and for an elasticity controlled fluid ($U_\lambda(t)$, Eq. 5). The different thinning regimes for viscoelastic solutions as discussed in the text are indicated with roman numeral I–V.

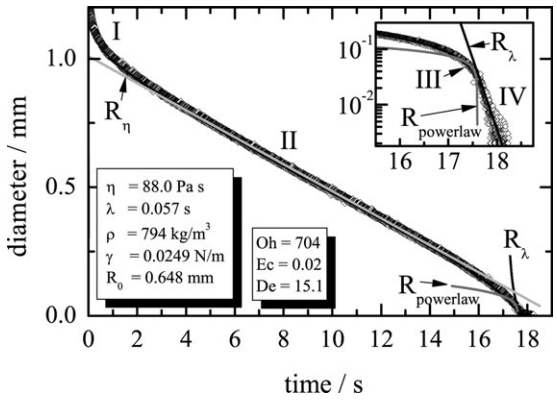

Figure 11. Evolution of the filament diameter for a weakly elastic fluid.

The evolution of R in a filament formed by a viscoelastic PIB in pristane solution from Figure 7 is compared to the predictions for a Newtonian fluid ($R_\eta(t)$, Eq. 18), a power law fluid ($R_{powerlaw}(t)$, Eq. 21), an elasticity-controlled fluid ($R_\lambda(t)$, Eq. 25). The different thinning regimes for viscoelastic solutions as discussed in the text are indicated with roman numeral I–V. The inset highlights on a logarithmic scale the onset of the finite extensibility limit in regime V.

initial state of stretch developed in the first regime and therefore can not be quantitatively predicted.

Given the interconnection of the several different thinning regimes for elasto-capillary numbers in the range of $0.5 < Ec < 4.7$, it is often not possible to derive an analytic description of the radius evolution of elastic fluid filaments connecting the drops. However, for $Ec \gg 4.7$ (and $Oh \gg 0.2$) it is often observed that regime IV, the elastic thinning regime, is dominating and setting in from the beginning of a dispensing operation. This is observed for the Boger fluid in the images of Figure 8, and captured with capillary breakup experiments in Figure 12. The filament life time can be estimated from Eq. 25 as

$$\Delta t_\lambda = 3\lambda \ln\left(\frac{R_0}{R_{\min}}\right) \tag{26}$$

To calculate the radius $R_{\min}$ at which the regime IV ends requires, in principle, information on the finite extensibility and the amount of prestretch that occurred in the nozzle. However, from experimental observations it can be concluded that at a $R_{\min} \sim 1$ μm the filament breaks quickly due to external influences and, therefore, $\Delta t_\lambda = 3\lambda \ln(R_0/1\ \mu m)$. The estimated breakup time is proportional to the relaxation time λ. For the PIB in PIB Boger fluid, Eq. 26 yields $\Delta t_\lambda = 500$ s which compares well to the experimentally observed breakup times (Figures 8 and 12). One further problem that can arise with these extremely long living and very thin filaments is the onset of evaporation effects that can even lead to solidifying fibers during a dispensing operation.[58]

The Dripping/Jetting Transition. The appropriate dynamic nondimensional number for elastic liquids ($Oh \gg 0.2$ and $Ec \gg 4.7$) is the Weissenberg number Wi. The dispensing in Figure 8 (of which a movie can be seen in the Supporting Information 'PIB in PIB - Wi = 5.11.avi') is with $Wi = 5.11$ still in the dripping regime. At higher-flow rates and $Wi = 51.1$ the dispensing is already in the jetting regime (as can be seen in the movie in the Supporting Information 'PIB in PIB - Wi = 51.1.avi'). The precise definition of an exact critical value of Wi for the transition is difficult. The effects of gravitational stretching are amplified due to the extreme longevity of the filaments. For the range of needle diameters in this study for flow rates below Wi of $O(15)$ the formation and falling of single droplets is still visible. The droplets are, however, still connected by the thin thinning filaments. For Weissenberg numbers of $O(20)$, the filament thins under its own weight and does not break into droplets. Subsequently, in a range of $20 < Wi < 40$ the diameter of this filament increases with flow rate. The onset of die-swell effects at higher flow rates increases the jet radius even above the nozzle radius.

Inviscid viscoelastic liquids

For viscoelastic solutions with low initial viscosity (or better: $Oh \ll 0.2$), the shape of the thinning curves is similar to the viscous counterparts. After an initial stabilization in regime I, one observes a fast, second, inertia controlled thinning regime described by Eq. 17 followed by the transition to an elastic regime IV. To determine if a transition to an elastic regime takes place, the intrinsic Deborah number De_0 should be calculated. [45] For $De_0 > 1$ the elastic thinning regime is dominating and determines the breakup time following Eq. 26. However, it should be noted that due to the proportionality of relaxation time and viscosity, for inviscid systems with $Oh \ll 0.2$ even a dominating elastic regime IV will not lead to very long breakup times. Therefore, inviscid viscoelastic liquids are generally easy to dispense.

One important aspect is the dependence of satellite droplet formation (and the resulting inaccuracy and spillage) on the Deborah number. As already stated above, the satellite droplet formation during the filament breaking process can be suppressed by increasing the viscosity above an Ohnesorge number of $Oh = 1$. However, for inviscid viscoelastic fluids with $Oh \ll 1$ the satellite droplet can also be suppressed by

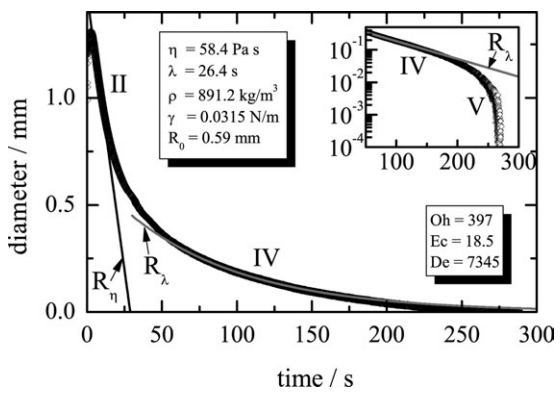

Figure 12. Evolution of the filament diameter for the thinning of a Boger Fluid.

The PIB in PIB fluid from Figure 8 (open symbols) is compared to the predictions for a Newtonian fluid ($R_\eta(t)$, Eq. 18), a power law fluid ($R_{powerlaw}(t)$, Eq. 21), an elasticity controlled fluid ($R_\lambda(t)$, Eq. 25). The dominant thinning regimes are indicated with the roman numerals II (initial Newtonian thinning) and IV (dominant elastic thinning). The inset highlights the onset of the finite extensibility limit in regime V on a logarithmic scale.

increasing the elastic component[59,60] and, therefore, the Deborah number above a critical value of $De > 0.2$.[44] A precise and clean dispensing without satellite droplets can, therefore, be achieved by the addition of traces of high-molecular weight polymers.

The Dripping/Jetting Transition. When the Deborah number is below its critical value $De_0 = 1$, the elasticity seems to suppress the chaotic dripping regime observed for low-viscosity Newtonian systems. The onset of jetting is preceded by a periodic oscillating movement of the detaching drop and oscillatory behavior of the droplet volume.[54] The Weber number as the appropriate dynamic nondimensional number above which only pure jetting is observed is still of order $We = O(1)$, however, similar to the Newtonian case this holds only for small nozzle radii.[54] For larger nozzle diameter, gravitational effects cannot be ignored and the mass of the leading drop is affecting the dynamics of the rest of the jet through a tension that is transmitted upstream along the viscoelastic jet. This regime has not yet been investigated. Similar to the viscous case, also for inviscid fluids with $De_0 > 1$ the critical transitional values for the Weissenberg number Wi are difficult to determine.

Conclusions

A set of model Newtonian, shear thinning and viscoelastic fluids that cover four orders of magnitude in viscosity and three orders of magnitude in elasticity (relaxation time) have been used to study the volumetric flow controlled dispensing under steady-state conditions. Difficulties in dispensing will occur when the breakup times of liquid filaments are long. In the dripping regime, filaments will then persist between the nozzle and the dispensed drop. In the jetting regime, such filaments connect the droplets developing in the fluid jet. Both situation will lead to spillage and inaccurate dosing. To identify such conditions, the thinning of liquid filaments and the effects of material properties on this phenomenon was used as a starting point. To predict the thinning and dispensing behavior of rheologically complex fluids, a set of material-property-based nondimensional groups, that is, the Ohnesorge, Deborah, and elasto-capillary number have been defined. Critical values of these nondimensional numbers allow one to identify the dominant mechanism resisting breakup (inertia, viscosity, or elasticity) and to predict the associated liquid filament life times. An operating space can thus be defined, which represent a ''map of misery'' and classifies fluids from easy to very difficult to dispense. For each of the thinning regimes nondimensional, dynamic numbers enable one to estimate the transition from a dripping to a jetting regime. The diagram of the operating space helps to anticipate problems when wanting to dispense rheologically complex fluids. However, the broad field of dispensing of complex fluids is not yet fully understood, in particular with regard to flow phenomena as deformation-thickening, yielding, thixotropy, or rheopexy, and requires more indepth experimental as well as computational studies to bring our understanding to the level of what is currently known about dispensing of Newtonian fluids.

Acknowledgments

PMP and JV acknowledge financial support from IWT (Vlaanderen). Dr. B. Molle and Dr. J. Paul from the Flamac Research Centre, Gent, Belgium are thanked for stimulating discussions on the role of dispensing in high throughput experimentation. CC and LjP acknowledge financial support of this project from the ERC-2007-StG starting grant 203043 NANOFIB.

Literature Cited

1. Derby B. Inkjet printing of functional and structural materials: fluid property requirements, feature stability, and resolution. *Annu Rev Mater Res*. 2010;40:395–414.
2. Cooper-White JJ, Fagan JE, Tirtaatmadja V, Lester DR, Boger DV. Drop formation dynamics of constant low-viscosity, elastic fluids. *J Non-Newtonian Fluid Mech*. 2002;106:29–59.
3. Morrison NF, Harlen OG. Viscoelasticity in inkjet printing. *Rheol Acta*. 2010;49:619–632.
4. Suryo R, Basaran OA. Local dynamics during pinch-off of liquid threads of power law fluids: Scaling analysis and self-similarity. *J Non-Newtonian Fluid Mech*. 2006;138:134–160.
5. Chen XB. Modeling and control of fluid dispensing processes: a state-of-the-art review. *Int J Adv Manuf Technol*. 2009;43:276–286.
6. Shin W, Nishibori M, Itoh T, Izu N, Matsubara I. Monitoring of dispensed fluid with the quartz crystal microbalance (QCM) for the better control of inkjet or dispenser machine. *J Ceram Soc Jpn*. 2008;116:459–461.
7. Li JP, Deng GL. *Technology development and basic theory study of fluid dispensing – a review*. In: *Proceedings of the Sixth IEEE CPMT Conference on High Density Microsystem Design and Packaging and Component Failure Analysis*. New York: IEEE, 2004.
8. Dogic Z, Fraden S. Development of model colloidal liquid crystals and the kinetics of the isotropic-smectic transition. *Philos Trans R Soc A:Math Phys Eng Sci*. 2001;359:997–1014.
9. Schultheisz CR, Leigh SJ. *Certification of the rheological behavior of SRM 2490, polyisobutylene dissolved in 2,6,10,14-tetramethylpentadecane*. In: *National Institute of Standards and technology special publication*, Vol. 262, p. 143. Gaithersburg. 2002.
10. Anna S, McKinley GH. Elasto capillary thinning and breakup of model elastic liquids. *J Rheol*. 2001;45:115–138.
11. Papageorgiou DT. On the breakup of viscous liquid threads. *Phys Fluids*. 1995;7:1529–1544.
12. Day RF, Hinch EJ, Lister JR. Self-similar capillary pinchoff of an inviscid fluid. *Phys Rev Lett*. 1998;80:704–707.
13. Chen AU, Notz PK, Basaran OA. Computational and experimental analysis of pinch-off and scaling. *Phys Rev Lett*. 2002;88:174501.
14. Tirtaatmadja V, McKinley GH, Cooper-White JJ. Drop formation and breakup of low viscosity elastic fluids: effects of molecular weight and concentration. *Phys Fluids*. 2006;18:043101.
15. Rodd LE, Scott TP, Cooper-White JJ, McKinley GH. Capillary break-up rheometry of low-viscosity elastic fluids. *ApplRheol*. 2005;15:12–27.
16. Entov VM, Hinch EJ. Effect of a spectrum of relaxation times on the capillary thinning of a filament of elastic liquid. *J Non-Newtonian Fluid Mech*. 1997;72:31–53.
17. Grant RP, Middleman S. Newtonian jet stability. *AIChE J*. 1966;12:669–678.
18. Kroesser FW, Middleman S. Viscoelastic jet stability. *AIChE J*. 1969;15:383–386.
19. Middleman S. *Modelling Axisymmetric Flows*. San Diego: Academic Pres, 1995.
20. McKinley GH. Visco-elasto-capillary thinning and break-up of complex fluids. *Rheol Rev*. 2005;1–48.
21. Chen XB, Kai J, Hashemi M. Evaluation of fluid dispensing systems using axiomatic design principles. *J Mech Design*. 2007;129:640–648.
22. Harkins WD, Brown FE. The determination of surface tension and the weight of falling drops. *J Am Chem Soc*. 1919;41:499–524.
23. Adamson A, Gast A. *Physical Chemistry of Surfaces*, 5th ed. New York: Wiley, 1997.
24. Zhang ZQ, Mori YH. Formulation of the Harkins-Brown correction factor for drop-volume description. *Ind Eng Chem Res*. 1993;32:2950–2952.
25. Yildirim OE, Xu Q, Basaran OA. Analysis of the drop weight method. *Phys of Fluids*. 2005;17:062107.
26. Bousfield DW, Keunings R, Marrucci G, Denn MM. Nonlinear-analysis of the surface-tension driven breakup of viscoelastic filaments. *J Non-Newtonian Fluid Mech*. 1986;21:79–97.
27. Clanet C, Lasheras JC. Transition from dripping to jetting. *J Fluid Mech*. 1999;383:307–326.
28. Brenner MP, Lister JR, Stone HA. Pinching threads, singularities and the number 0.0304. *Phys of Fluids*. 1996;8:2827–2836.

29. Henderson D, Segur H, Smolka LB, Wadati M. The motion of a falling liquid filament. *Phys Fluids*. 2000;12:550–565.
30. McKinley GH, Tripathi A. How to extract the Newtonian viscosity from capillary breakup measurements in a filament rheometer. *J Rheol*. 2000;44:653–670.
31. Pozrikidis C. Capillary instability and breakup of a viscous thread. *J Eng Math*. 1999;36:255–275.
32. Eggers J, Villermaux E. Physics of liquid jets. *Rep Prog Phy*. 2008;71:036601.
33. Sauter US, Buggisch HW. Stability of initially slow viscous jets driven by gravity. *J Fluid Mech*. 2005;533:237–257.
34. Eggers J. Universal pinching of 3D axisymmetrical free-surface flow. *Phys Rev Lett*. 1993;71:3458–3460.
35. Basaran OA. Small-scale free surface flows with breakup: drop formation and emerging applications. *AIChE J*. 2002;48:1842–1848.
36. Lister JR, Stone HA. Capillary breakup of a viscous thread surrounded by another viscous fluid. *Phys Fluids*. 1998;10:2758–2764.
37. Rothert A, Richter R, Rehberg I. Transition from symmetric to asymmetric scaling function before drop pinch-off. *Phys Rev Lett*. 2001;8708:084501.
38. Doshi P, Suryo R, Yildirim OE, McKinley GH, Basaran OA. Scaling in pinch-off of generalized Newtonian fluids. *J Non-Newtonian Fluid Mech*. 2003;113:1–27.
39. Kowalewski TA. On the separation of droplets from a liquid jet. *Fluid Dyn Res*. 1996;17:121–145.
40. Notz PK, Chen AU, Basaran OA. Satellite drops: unexpected dynamics and change of scaling during pinch-off. *Phys Fluids*. 2001;13:549–552.
41. Ambravaneswaran B, Subramani HJ, Phillips SD, Basaran OA. Dripping–jetting transitions in a dripping faucet. *Phys Rev Lett* 2004;93:034501.
42. Brenner MP, Shi XD, Nagel SR. Iterated instabilities during droplet fission. *Phys Rev Lett*. 1994;73:3391–3394.
43. Henderson DM, Pritchard WG, Smolka LB. On the pinch-off of a pendant drop of viscous fluid. *Phys Fluids*. 1997;9:3188–3200.
44. Bhat PP, Appathurai S, Harris MT, Pasquali M, McKinley GH, Basaran OA. Formation of beads-on-a-string structures during breakup of viscoelastic filaments. *Nat Phys*. 2010;6:625–631.
45. Campo-Deano L, Clasen C. The slow retraction method (SRM) for the determination of ultra-short relaxation times in capillary breakup experiments. *J Non-Newtonian Fluid Mech*. 2010;165:1688–1699.
46. Yildirim OE, Basaran OA. Dynamics of formation and dripping of drops of deformation-rate-thinning and -thickening liquids from capillary tubes. *J Non-Newtonian Fluid Mech*. 2006;136:17–37.
47. Bhattacharjee PK, Nguyen DA, McKinley GH, Sridhar T. Extensional stress growth and stress relaxation in entangled polymer solutions. *J Rheol*. 2003;47:269–290.
48. Clasen C. Capillary breakup extensional rheometry of semi-dilute polymer solutions. *Korea-Australia Rheol J*. 2010;22:331–338.
49. Arnolds O, Buggisch H, Sachsenheimer D, Willenbacher N. Capillary breakup extensional rheometry (CaBER) on semi-dilute and concentrated polyethyleneoxide (PEO) solutions. *Rheol Acta*. 2010;49:1207–1217.
50. Bhattacharjee PK, Oberhauser JP, McKinley GH, Leal LG, Sridhar T. Extensional rheometry of entangled solutions. *Macromolecules*. 2002;25:10131–10148.
51. Yesilata B, Clasen C, McKinley GH. Nonlinear shear and extensional flow dynamics of wormlike surfactant solutions. *J Non-Newtonian Fluid Mech*. 2006;133:73–90.
52. Clasen C, Plog JP, Kulicke WM, Owens M, Macosko C, Scriven LE, Verani M, McKinley GH. How dilute are dilute solutions in extensional flows? *J Rheol*. 2006;50:849–881.
53. Plog JP, Kulicke WM, Clasen C. Influence of the molar mass distribution on the elongational behaviour of polymer solutions in capillary breakup. *Appl Rheol*. 2005;15:28–37.
54. Clasen C, Bico J, Entov VM, McKinley GH. 'Gobbling drops': the jetting–dripping transition in flows of polymer solutions. *J Fluid Mech*. 2009;636:5–40.
55. Miller E, Clasen C, Rothstein JP. The effect of step-stretch parameters on capillary breakup extensional rheology (CaBER) measurements. *Rheol Acta*. 2009;48:625–639.
56. Goldin M, Yerushalmi J, Pfeffer R, Shinnar R. Breakup of a laminar capillary jet of a viscoelastic fluid. *J Fluid Mech*. 1969;38:689–711.
57. Mun RP, Byars JA, Boger DV. The effects of polymer concentration and molecular weight on the breakup of laminar capillary jets. *J Non-Newtonian Fluid Mech*. 1998;74:285–297.
58. Sattler R, Wagner C, Eggers J. Blistering pattern and formation of nanofibers in capillary thinning of polymer solutions. *Phys Rev Lett*. 2008;100:164502.
59. Christanti Y, Walker LM. Surface tension driven jet break up of strain-hardening polymer solutions. *J Non-Newtonian Fluid Mech*. 2001;100:9–26.
60. Christanti Y, Walker LM. Effect of fluid relaxation time of dilute polymer solutions on jet breakup due to a forced disturbance. *J Rheol*. 2002;46:733–748.

Manuscript received Feb. 4, 2011, and revision received Oct. 27, 2011.